Structural Analysis and Photocurrent Spectroscopy of CCCs on 99.99% Aluminum

F. Di Quarto,[a,*,z] M. Santamaria,[a] N. Mallandrino,[a] V. Laget,[b] R. Buchheit,[b,*] and K. Shimizu[c]

[a]*DICPM-Facoltà di Ingegneria, Università di Palermo, 90128 Palermo, Italy*
[b]*Department of Material Science and Engineering, Ohio State University, Columbus, Ohio, USA*
[c]*University Chemical Laboratory, Keio University, 4-1-1 Hiyoshi, Yokohama 223, Japan*

A characterization of chromate conversion coatings (CCCs) formed in the presence and in the absence of accelerator (ferro-ferricyanide redox couple) has been performed by various techniques (transmission electron microscopy, TEM, glow discharge optical emission spectrometry, GDOES, X-ray absorption near-end structure, XANES, and photon correlation spectroscopy). The results of a detailed investigation on morphological, compositional, and solid-state properties of freshly converted aluminum samples at different immersion times (30 s-90 min) are reported. The TEM and GDOES data suggest the presence of iron-cyanide species only in the external layer of CCC of nearly constant thickness. The XANES data suggest the presence of both Cr(VI) and Cr(III) species with a ratio Cr(VI)/Cr(III) close to 1:2. This ratio remains constant with the conversion time and seems slightly affected by the composition of conversion solution. The photoelectrochemical study suggests an insulating or slightly p-type behavior for CCC layers. A bandgap value of about 2.55 eV has been estimated, regardless of the conversion solution, although some differences in the photocurrent spectra have been observed for coatings formed in the presence or absence of accelerator. The location of electronic energy levels of the Al/CCC/electrolyte interface has been derived which could account for the different kinetics of coating formation in the presence of accelerator.
© 2003 The Electrochemical Society. [DOI: 10.1149/1.1602081] All rights reserved.

A large research effort has been devoted in the last years to the understanding of the exact nature of the chromate conversion coating (CCC) and its mechanism of protection against corrosion of aluminum metal and alloys.

Surface analysis techniques have revealed that the composition of the coatings depends on the nature of the chemical conversion bath.[1-3] It is now agreed that the coatings are amorphous[2,3] and that both Cr(III) and Cr(VI) species are incorporated into the films, with possible formation of a mixed Cr(III)-Cr(VI) oxide as suggested by recent Raman spectroscopy analysis.[4,5]

The mechanism of action of chromate in assuring the protection against pitting corrosion is still under debate. From this point of view a large interest exists in understanding the influence of aging on the protection action of CCCs. It has been shown that long-term or temperature aging acts on the mechanism of release of Cr(VI) species so affecting the ''active protection'' of CCCs also called self-healing. In this frame different hypothesis have been suggested to explain the associated loss of corrosion protection.[5-9] Among those, structural changes occurring into the CCC and related to dehydration were evidenced.[10]

As for the mechanism of formation and growth of CCCs only very few papers have addressed both the role of the redox couples, usually added to the commercial conversion bath to speed up the growth of the coating, and the mechanism of initial formation of CCCs during the conversion process.[3,4]

Brown *et al.*[3] suggested that on a very pure Al surface a uniform coating develops due to a mechanism of electron tunneling injection through the chemically thinned alumina films always present on aluminum metal. This hypothesis could account only for the very first instants of formation of CCC and the authors did not account for the growth of thicker coatings as occurring in long lasting immersion experiments. We believe that both the role of the various redox couples in accelerating the coating growth and the mechanism of growth itself require a better knowledge of the solid-state properties and morphology of thick CCCs grown on well defined Al surface.

In order to gain a better understanding of these different aspects, we have undertaken a photocurrent spectroscopy (PCS) study of different conversion coatings grown on pure Al surfaces.[11]

* Electrochemical Society Active Member.
z E-mail: diquarto@mbox.unipa.it

In this paper we report the results of a detailed study on composition, morphology, and solid-state properties (optical bandgap E_g, flatband potential V_{FB}) of CCCs grown both in the presence and in the absence of accelerator (ferricyanide) using both nonelectrochemical (X-ray absorption near-edge structure, XANES, glow discharge optical emission spectrometry, GDOES, and transmission electron microscopy, TEM) and photo-electrochemical (PCS) analytical techniques. The role of the ferricyanide redox couple in speeding up the growth rate of the coatings is discussed on the basis of the solid-state properties of CCC. A quantitative PCS study of the dependence of the optical bandgap values on the composition of the coatings is suggested in agreement with the chromium(VI) content and the hydration degree respectively determined by XANES and thermoanalysis.

On the basis of PCS analysis, the composition of a fresh CCC is derived which appears compatible with the compositional analysis derived by other techniques. These results will be used in future works to monitor *in situ* by PCS technique possible changes in solid-state properties of CCCs, grown on Al and its alloys, as a function of aging process.

Experimental

Al foils 99.99% (Si 4.9, Fe 1.9, Cu 3.0, Mg 3, and other metals <1 part per million, ppm) of purity (WAV-Berlin) have been used. Specimens were electrochemically polished (EP) for 5-10 min at 20 V in an ethanol/HClO$_4$ solution (1/4 v/v) at *ca.* 5°C, rinsed in distilled water, and then immersed in the conversion bath. After the coating process, the specimens were sealed to have a limited surface exposed to the solution and left in the laboratory atmosphere for different times. Specimens investigated after less than 24 h of aging in the laboratory atmosphere will be identified as ''fresh'' electrodes.

CCCs have been formed on EP-Al samples in a solution containing 4 g/L CrO$_3$, 3.5 g/L Na$_2$Cr$_2$O$_7$; 0.8 g/L NaF solution (pH 1.7) at room temperature, for immersion times usually ranging between 5 and 300 s. The same solution was also used in presence of accelerator [1 g/L K$_3$Fe(CN)$_6$] for the same conversion times. CCC without ferricyanide (CCC-wof) was used for first type of coatings, whereas CCC-wf (with ferricyanide) was used for the second type of coatings.

Chemically etched aluminum samples (CE-Al) were also prepared by immersion for 2 min in an alkaline bath (0.1 M NaOH) at 65°C. After rinsing in water, samples were immersed for 3 min in an acid bath, (commercial Sanchem 1000 bath) at 55°C, rinsed in dis-

tilled water, and finally converted in chromate baths for different times.

The photoelectrochemical investigation was performed in quasi-neutral solutions of 0.5 M K_2SO_4 (pH 6) unless differently stated. All solutions were held in contact with air. The setup used for photoelectrochemical investigation has been described elsewhere.[12] The photocurrent spectra were obtained by correcting the raw photocurrent data for the efficiency of a lamp-monochromator system measuring the photon number by an Eppley thermopile at every 5 nm.

XANES and chemical analysis.—XANES measurements were performed at the Chromium K edge (5989 eV) at the National Synchrotron Light Source, Brookhaven Laboratory on beamline X10C. Fresh samples were measured directly recording X-ray fluorescence in a similar way to what reported previously.[10] The height of the absorption edge is proportional to the amount of Cr in the radiated volume and consequently of the coating thickness. After normalization of the spectra, a good estimation of Cr(VI)/total Cr is given by the height of the pre-edge peak. XANES measurements were performed on CCCs grown on both EP-Al and CE-Al samples.

Chemical analysis was performed on powder coating after stripping from CE-Al substrate by dipping for 5-30 s in a 5 vol % HNO_3 solution as described in Ref. 13. This short treatment allowed loosening bonds between coating and Al substrate. The sample was then dipped in deionized (DI) water under vigorous stirring and the coating which separates easily from substrate was filtered, rinsed, with alcohol and let to dry, then dissolved in hot acid to be measured by inductively coupled plasma-atomic emission spectroscopy (ICP-AES).

In the following, all quantitative analysis (XANES, ICP-AES, energy dispersive X-ray analysis, EDX,) data are reported considering metallic cations only.

TEM-EDX analysis.—The CCC films were stripped from the EP-Al substrate using a mercuric chloride ($HgCl_2$) solution, rinsed thoroughly in distilled water, and finally, collected onto copper grids. Ultramicrotomed sections of the aluminum substrate and CCC films were prepared in the usual manner using an RMC XL ultramicrotome.[3] After encapsulation in a resin polymerizing at 60°C, specimens were trimmed initially with a glass knife and suitably thin sections, about 10 nm thick, prepared by sectioning in a direction approximately parallel to the metal/film interface with a diamond knife. The stripped films and ultramicrotomed sections were examined in a TECNAI F20 field-emission, ultra-high resolution transmission electron microscope operated at 200 kV. When EDX analysis was necessary, an electron probe of about 5 nm diam was used to optimize spatial resolution and X-ray count rate. The microscope was equipped with Gatan imaging filtering system (GIF); electron-energy-loss imaging of Fe was carried out using the FeL2,3 loss peak at 708 eV.

RF-GDOES.—The CCC films were depth profiled using a Jobin-Yvon RF 5000 instrument. The CCC-coated aluminum foils were stuck onto rigid aluminum plates by adhesive and, subsequently, placed in a specimen holder that was made a cathode. The CCC films were sputtered with an argon pressure of 0.31 Torr by applying a radio frequency (rf) of 13.56 MHz and 40 W power. Light emission of characteristic wavelengths, associated with the excited atomic species, was monitored throughout the analysis with a sampling time interval of 0.01 s. The relevant wavelengths (nm) were as follows: Al, 396.15; H, 121.57; Cr, 425.43; C, 156.14; Fe, 385.99; N, 149.26; and O, 130.22.

Results

Morphological and compositional study.—The morphology of CCCs grown on CE-Al and Al alloys has been frequently investigated by scanning electron microscope (SEM) so that these data will be omitted in this study. Previous SEM studies have invariably shown a cracked mud structure at the surface of a CCC sample observed also by us at longer conversion times. At shorter times
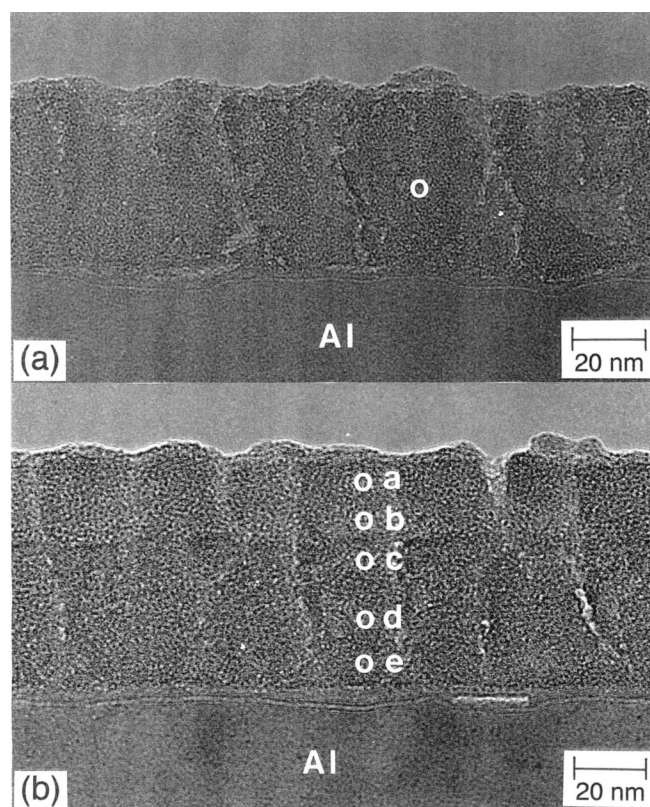

Figure 1. Transmission electron micrograph of an ultramicrotomed section of electropolished aluminum substrate and CCC film formed by 30 s immersion in acid chromate solution (a) without ferricyanide and (b) with ferricyanide. Probe positions are also indicated where EDX analysis was carried out. Probe size employed was about 5 nm in diam to optimize count rate and spatial resolution.

(lower than 5 min) or in the absence of ferricyanide, the surface of EP-Al samples appeared smoother with a preferential growth of CCCs at the grain boundary regions.

In Fig. 1 we report the ultramicrotomed section of an EP-Al sample after 30 s of conversion in chromate baths without and with ferricyanide (Fig. 1a and b). In the case of CCC-wf, a close inspection evidenced the presence of a duplex structure with a lighter (less dark) external region (about 25 nm thicker) at the solution/CCC interface showing a slightly coarser texture. For CCC-wof, a homogeneous single layer is evidenced in Fig. 1a.

For both samples, a third layer was observed at still higher magnifications at the metal/CCC interface (see Fig. 2a). As previously suggested by others,[3] this very thin layer (in the order of 0.6 nm as measured in Fig. 2b) could have been a residual aluminum oxide layer still covering the metal substrate after the electropolishing procedure and conversion process.[11]

Figure 2a seems to indicate that the CCC film exhibited a considerable coarse texture suggesting nanocolloidal particles of hydrated chromium oxides. Lattice fringes of spacing 0.234 nm, corresponding to (111) crystallographic planes of aluminum substrate, are observed clearly in the same figure.

EDX measurements performed at the points marked a-e in Fig. 1b revealed the presence of iron species (about 20 atom % from instrumental quantitative analysis) only in the lighter regions (a, b points). Iron species were absent in regions marked by c, d, e. A presence of iron on the external region of CCC-wf as well as at the surface of very thin tunnels, into the otherwise compact structure of the coating, is evidenced in Fig. 3. In such a figure, the no-loss image and the Fe_{L2-3} loss image of a sample converted for 2 min
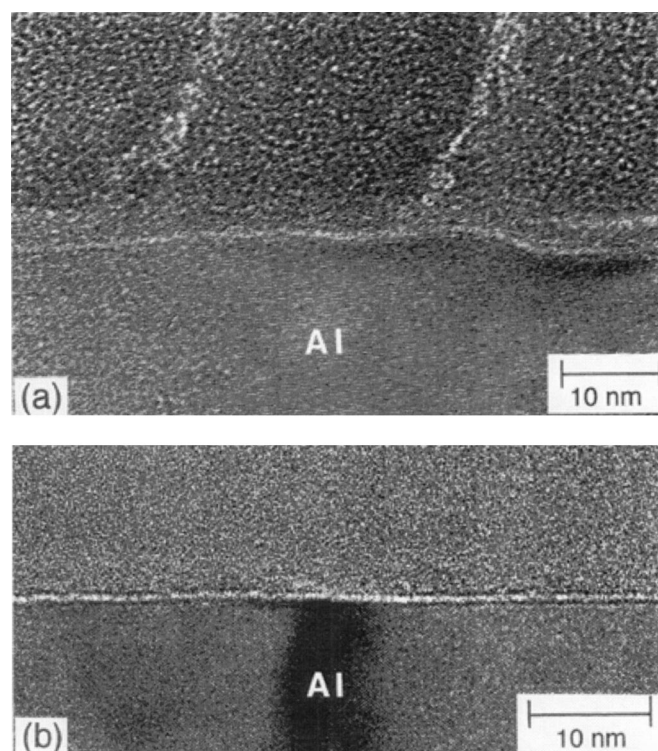
Figure 2. High resolution transmission electron micrographs of: (a) the aluminum/CCC film interface relating to film of Fig. 1b; (b) aluminum/anodic alumina interface.

are reported. The presence of such tunnels into the structure of the coatings is also observed in CCC-wof.

In Fig. 4 we report the CCC thickness *vs.* the square root of conversion time for samples converted for different times (0.5, 2, and 5 min) in the presence and in the absence of accelerator. As previously anticipated and in agreement with the XANES data (see below), a higher slope was obtained for EP-Al samples converted in the presence of ferricyanide (faster growth).

Further qualitative information on the CCC composition was also obtained from GDOES analysis of samples converted in the presence and in the absence of ferricyanide. In Fig. 5 we report the GDOES spectrum of a CCC converted for 2 min showing the absence of any appreciable amount of Al species in the external region while the presence of Al species cannot be excluded in the inner part of a CCC. When ferricyanide was used in the coating bath, a weak signal related to the presence of Al species was observed during all the sputtering time (compare Fig. 5 and Fig. 6). Although the comparison of the two spectra seems to suggest that such small amount of Al could be incorporated into the CCC, we cannot exclude that the Al signal comes from entrapped electrolyte solution. In the case of CCC-wf, the presence of iron species on the external part of the conversion layer is confirmed also by GDOES spectra, which show a large peak at low sputtering times followed by a plateau at longer times.

The intensity of nitrogen signal (not reported here) is following the same variation showing that iron atoms are still present under ferricyanide form in the CCC.

A more quantitative analysis of Al and Fe species contained into the CCC was performed by ICP-AES on stripped CCC samples. From such studies we obtained an average concentration of about 7 atom % for iron in the case of CCC-wf. As for the Al content, an average value of 1 atom % and 4 atom % was measured for CCC-wf and CCC-wof, respectively.

The presence of both Cr(III) and Cr(VI) species into a CCC is very well known in the literature of CCC. However, the ratio of the
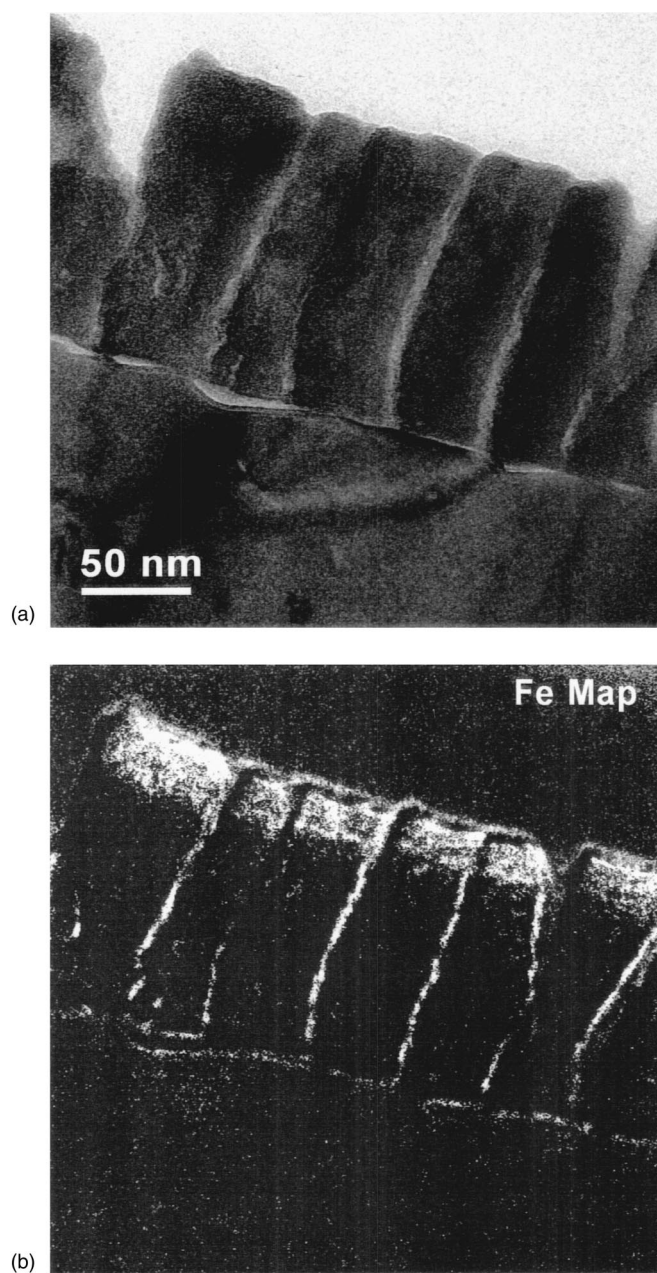

Figure 3. (a) No loss image of a 2 min CCC grown in the presence of ferricyanide; (b) $Fe_{1,2,3}$ loss image showing iron distribution in the film.

two species depended on various parameters, so we performed XANES analysis on samples prepared by different surface treatments (chemical etching and electropolishing) and immersed for different conversion times in both types of conversion baths.[4-10]

Fig. 7 and 8 show the results of XANES measurements on CE-Al samples and allow evaluation of the influence of ferricyanide and of the coating time on the coating thickness and the Cr(VI) content. For a 3 min coating time, the coating was 2.5 times thicker with ferricyanide than without. After normalization, the Cr(VI)/Cr total ratio is calculated to be lower for CCC-wf (35%) than CCC-wof (38%). Both these values are averaged over 5 samples for conversion times between 1 and 4 min. Figure 7 shows that both Cr(VI) and Cr(III) species are incorporated into CCC at almost constant ratio in all the range of coating times investigated.

Comparing these results to those obtained on EP-Al samples (not shown) reveals the importance of the surface preparation: in the second case, the increase of thickness is in the order of 1.4 only
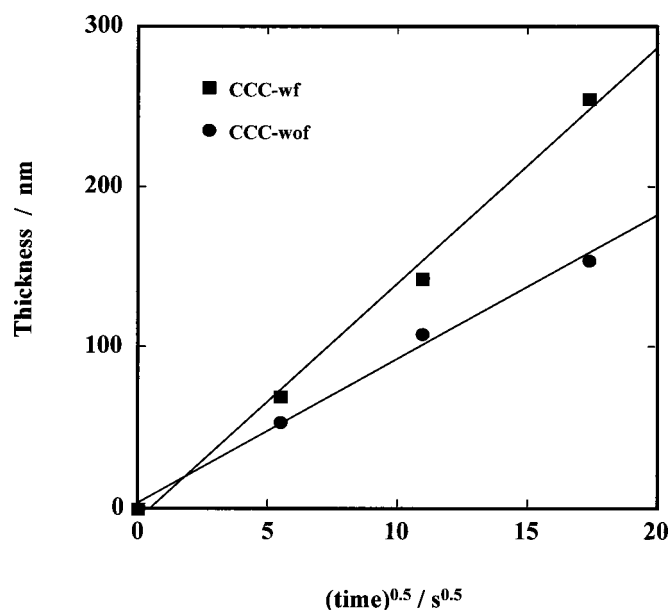
Figure 4. Thickness of CCC grown on electropolished aluminum substrate measured by TEM of ultramicrotomed cross sections as a function of (conversion time)$^{0.5}$.

Figure 6. GDOES spectrum relating to a 2 min CCC-wf.

(average value) and slightly lower Cr(VI) contents are obtained (32.7% wf, and 37.5% wof, averaged values as above).

Figure 9 shows the variation with coating time of chromium content [total and Cr(VI) species] in CCC-wof on CE-Al. Both curves follow the same dependence on the conversion time in the overall explored time region; when the data were plotted as a function of (time)$^{0.5}$, they could be interpolated linearly with a very good correlation coefficient (see Fig. 9); both lines intersected the time axis at a large positive value of time ($t_0 = 16$ s), in agreement with the hypothesis that a different growth mechanism controlled the coating growth at shorter times.

The same time dependence were obtained on EP-Al samples for conversion time up to 5 min although with slightly lower correlation coefficients ($R^2 = 0.98$) if compared with the value of Fig. 9 for CE-Al samples ($R^2 = 0.993$). Different axis intercepts and lower growth rates (slopes) were observed in the absence of ferricyanide (see above).
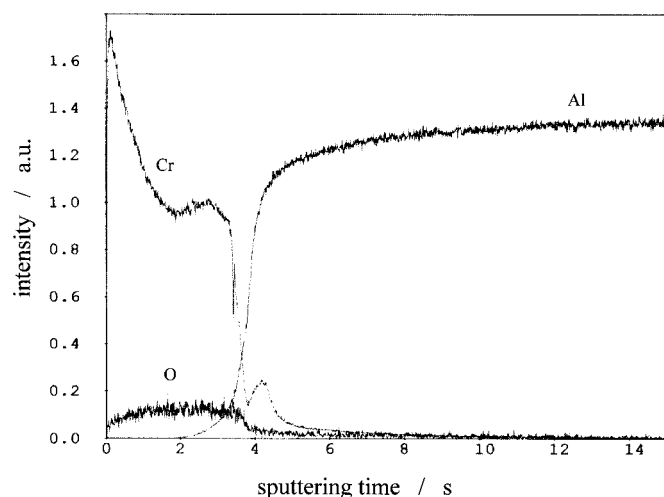
PCS study.—In a previous work[11] we presented some preliminary results on the photoelectrochemical behavior of CCCs showing an influence of the electrode potential on the optical bandgap measured under different experimental conditions.

The origin of this influence was not investigated in depth, although it was clearly shown that in some cases it could be related to the onset of an external electron photoinjection process from the Al substrate to the electrolytic solution. Such a process is not surprising if we take into account both the very extreme thinness of the oxide layer (around 2 nm) covering the Al surface after the electropolishing process and the very good photoemitting properties of aluminum in contact with electrolytic solutions.[14,15]

On the other hand it is also known from previous PCS studies that the photocurrent yield of passive chromium and bulk chromium oxides[16,17] is very low under cathodic or anodic polarization. This means that in the case of cathodic photocurrent we need to discriminate between the existence of different light absorption processes all contributing, eventually, to the measured photocurrent (see Fig. 10):

(*i*) Interband bulk excitation in a CCC due to the absorption of incident photons $[h\nu > (E_g)^{film}]$ generating mobile electron-hole couples.
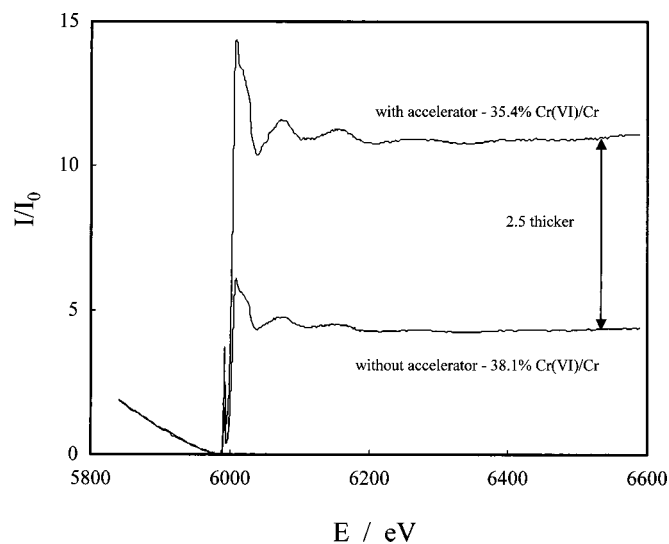

Figure 5. GDOES spectrum relating to a 2 min CCC-wof.

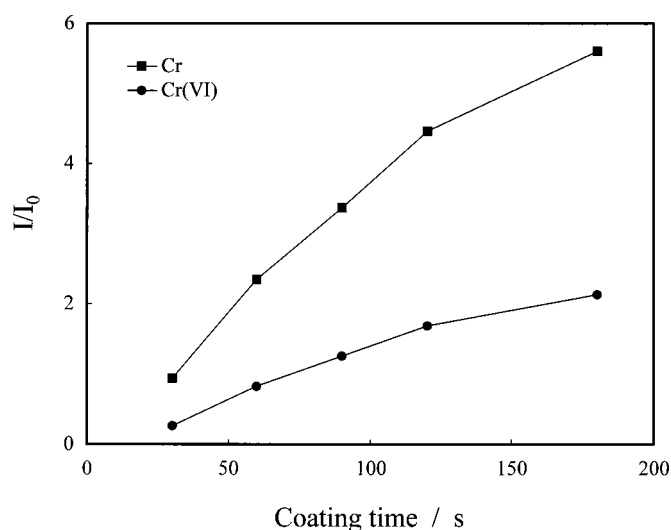**Figure 7.** XANES data relating to CCC grown for 3 min on 99.99% Al chemically etched.

Figure 8. Cr and Cr(VI) content in CCC grown on 99.99% chemically etched Al in the absence of ferricyanide as a function of the conversion time.

Figure 10. Different light absorption processes originating cathodic photocurrent: (a) interband bulk excitation; (b) internal electron injection process; (c) external electron photoemission from Al substrate to the solution.

(*ii*) Internal electron injection process from the metal Fermi level to the oxide conduction band. This process is possible in the presence of slightly absorbing insulating films or thin, not heavily doped, p-type semiconducting films and it could account for a part of the cathodic photocurrent due to the impinging photons reaching the metal/oxide interface.

(*iii*) External electron photoemission from Al substrate to the solution, in areas of electrode surface where a direct contact through tunnels exists between the electrolytic solution and the very thin native oxide allowing a tunneling process of electrons from the underlying metal to the acceptor species into solutions (see scheme in Fig. 10).

These processes follow different theoretical dependencies from the energy of incident photons and electrode potential (Ref. 11, 12, 14, and 18) and they have been investigated for identifying the origin of measured photocurrent. In the case of fresh CCCs formed for immersion times longer than 30 s, a detailed study of the dependence of cathodic photocurrent from photon energy and electrode
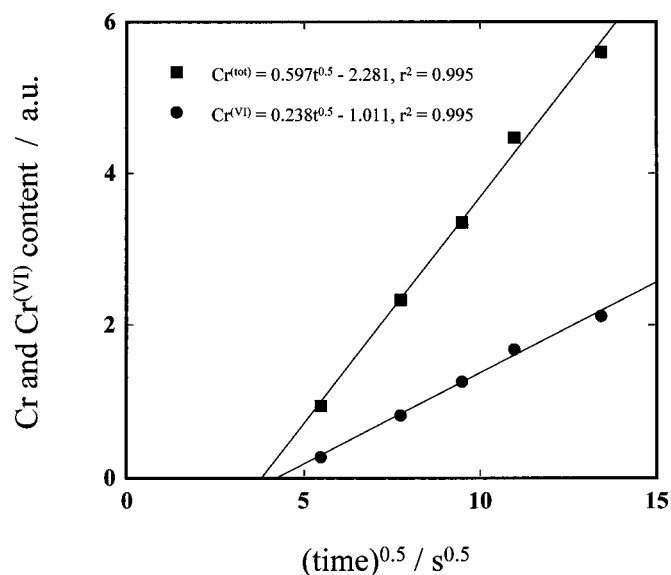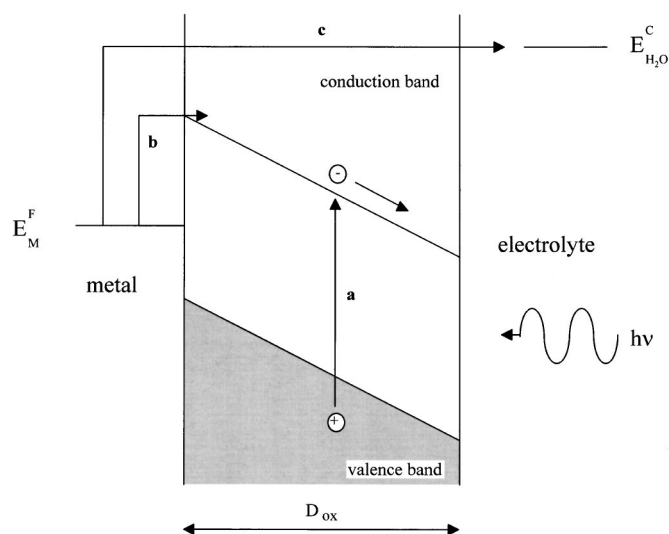

Figure 9. Cr and Cr(VI) content in CCC grown in the absence of ferricyanide on chemically etched Al samples *vs.* (conversion time)$^{0.5}$. Data from Fig. 8.

potential allowed to exclude as a source of the measured photocurrent any internal or external photoemission process.

The large bandgap (>6.3 eV) of Al_2O_3 on EP-Al as well as the extreme thinness of the residual oxide (0.6 nm) at metal/CCC inner boundary exclude any contribution from such interlayer to the measured photocurrent. Accordingly, the optical excitation process in the oxide is omitted in Fig. 10.

In order to use PCS analysis in a quantitative way for the characterization of coatings formed for different immersion times and in different conversion baths, the coatings were characterized in the same solution (0.5 M K_2SO_4) and by following the same procedure. At this aim we have chosen to characterize CCC at the initial corrosion potential, U_{corr}, and at a second constant potential more cathodic than the U_{corr} initial values.

As U_{corr} values of different electrodes usually ranged between -1 V/saturated calomel electrode (SCE) and -1.28 V/SCE, after different initial preparations, the comparison of photocurrent spectra was made at an initial electrode potential $U_E = -1.30$ V/SCE in 0.5 M K_2SO_4 solution.

In Fig. 11 we report the normalized photocurrent spectra, corrected for the lamp emission (photocurrent yield), relative to EP-Al samples, before the conversion process, and to 5 min CCC grown with and without accelerator. As evidenced in Fig. 11, the photocurrent spectra of coated EP-Al samples differed greatly from that of bare EP-Al sample because of the onset of a large photocurrent contribution in the region of wavelengths around 300 nm. It has been reported that photocurrent spectra of chromium oxides passive films show maxima[16,17] in the same wavelength range.

By assuming the presence of nondirect (indirect for crystalline materials) optical transitions between valence band (VB) and conduction band (CB) of a CCC, and a direct proportionality between the photocurrent yield, I_{ph}, (see above) and the light absorption coefficient α,[12] the following equation holds

$$I_{ph}h\nu = \text{const}(E_g - h\nu)^2 \qquad [1]$$

valid for photon energies close to E_g. The optical bandgap of an amorphous CCC can be estimated by extrapolating to zero the $(I_{ph}h\nu)^{0.5}$ *vs.* $h\nu$ plots, as shown in Fig. 12 and 13 for CCC-wof after different conversion times (5 min and 90 min). In Table I we report the bandgap values of fresh (see experimental) CCCs grown for different conversion times (30 s-60 min) with and without accelerator.
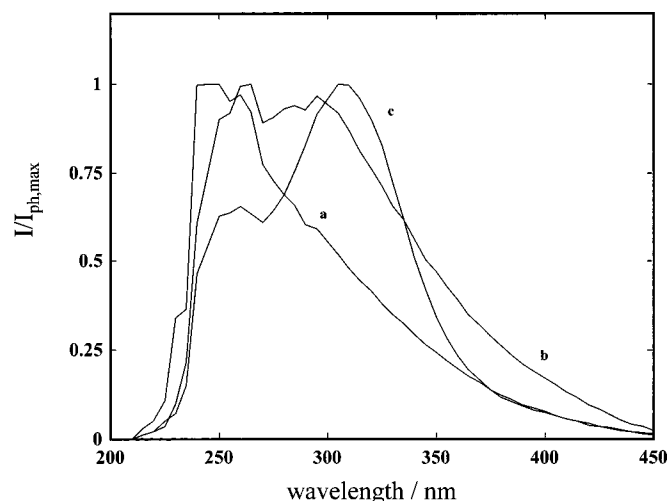
Figure 11. Normalized photocurrent action spectra corrected for the lamp efficiency, recorded by polarizing the electrodes in 0.5 M K_2SO_4 at $U_e = -1.3$ V/SCE, relating to: (a) nonconverted EP Al; (b) EP-Al after 5 min of conversion in the presence of accelerator; and (c) EP-Al after 5 min of conversion without accelerator.

Figure 13. Photocurrent action spectrum corrected for the lamp efficiency, relating to 90 min CCC-wof on EP-Al, polarized in 0.5 M K_2SO_4 at $U_e = -1.3$ V/SCE. Inset: bandgap determination by assuming nondirect optical transitions.

As a first approximation, by taking into account the results of Table II relative to samples analyzed at the most negative potentials (between -1.5 and -1.3 V/SCE), we will assume for fresh CCC-wof an average optical bandgap of 2.55 ± 0.05 eV. The amorphous nature of the CCC and the field dependence of the quantum yield in low mobility materials could help to explain the relatively large dependence of the optical bandgap values of a CCC at more positive electrode potentials ($-1.20 \leq U_E \leq -1.05$ V/SCE).

We stress that from the same plots (Fig. 12 and 13) it is possible to derive, from the higher photon energies region ($h\nu > 3.40$ eV), a second extrapolation which gives bandgap values at around 3.0 eV ± 0.1 eV. It may be interesting to recall that photocurrent spectra showing similar behavior but slightly different optical bandgap values ($E_g = 2.55$-2.95 eV) have been reported in the literature for passive films grown on Cr metal at more anodic electrode potential.[16,17]

Note that higher photocurrent values (but always in the range of nanoamperes) were usually measured for CCC films of lower thickness (or shorter conversion times) at constant potential and wavelengths.

This fact together with the presence in the photocharacteristics (see Fig. 14) of a frequently observed photocurrent inversion, from cathodic to anodic values on going toward anodic potentials, suggests that CCCs usually behave like insulators (Fig. 14) (or as slightly doped, in some cases, p-type semiconductors Fig. 15). This behavior is also reminiscent of analogous behavior of Cr passive films.[16,17]

In order to determine the flatband potential, V_{FB}, for the different films we used two different approaches depending from the fact that the blocking region of the I_{tot} vs. U_E plots was more or less wide. In fact in some cases the inversion photocurrent potential was accessible by recording the I_{ph} vs. U_E plots at different λ, before the increase of the total current (see Fig. 14) made impossible to observe the inversion photocurrent potential. In some other cases, when the inversion potential was not accessible or missing, we used the zero photocurrent potential value V^*, obtained by extrapolating to zero the $(I_{ph})^n$ vs. U_E plots, as a measure of the flatband potential (see Fig. 15).

As a general trend we observed that in the presence of strongly absorbed light the inversion photocurrent potential values were more anodic. Such a trend was observed also for the V^* derived from the best fitting of $(I_{ph})^n$ vs. U_E plots with n values usually less than one (supralinear photocharacteristics were usually recorded) and slightly increasing with increasing photon energies. For these reasons the estimated flatband potentials of CCC derived from the photocharacteristics should be taken with some caution.
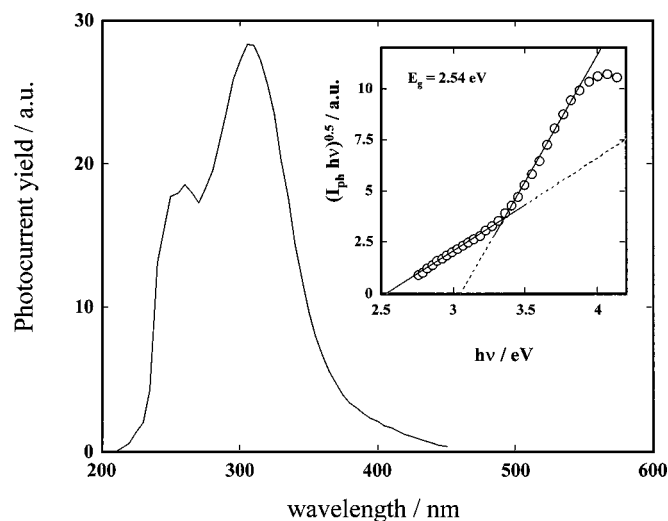

Figure 12. Photocurrent action spectrum corrected for the lamp efficiency, relating to 5 min CCC-wof on EP-Al, polarized in 0.5 M K_2SO_4 at $U_e = -1.3$ V/SCE. Inset: bandgap determination by assuming nondirect optical transitions.
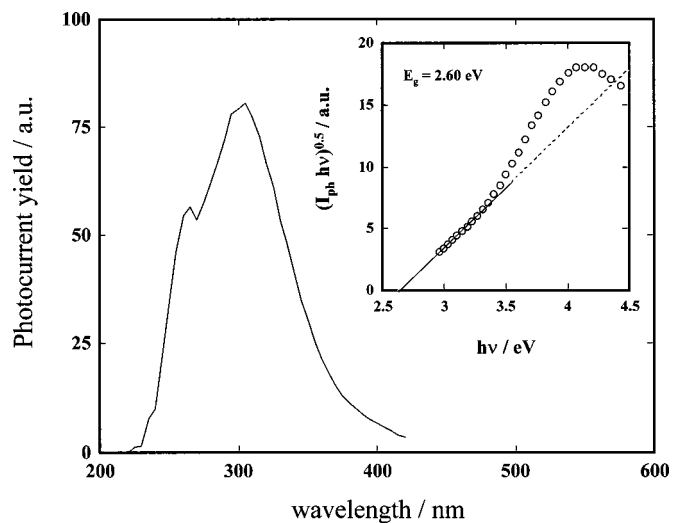
Table I. Bandgap values of CCC as a function of the conversion time at $U_E = -1.3$ V/SCE in 0.5 M K_2SO_4.

Conversion time (min)	CCC-wf E_g (eV)	CCC-wof E_g (eV)
0.5	2.60	2.60
1	2.53	2.52
2	2.57	2.58
5	2.54	2.54
60	2.59	2.58

Table II. Bandgap values relative to fresh 5 min CCC-wof, estimated by assuming non-direct optical transitions, as a function of the electrode potential in 0.5 M K$_2$SO$_4$.

U_e/V(SCE)	−1.50	−1.30	−1.20	−1.05
E_g/eV	2.51	2.54	2.67	2.86

At fixed wavelength (λ = 300 nm), the inversion photocurrent potential (U_{inv} = +0.10 V/normal hydrogen electrode, NHE) for specimen showing an insulating-like behavior was about 0.15 V more cathodic of the zero photocurrent potential (V^* = +0.28 V/NHE) of CCC showing a p-type-like behavior (see Fig. 14 and 15a). According to this finding we roughly assumed a flatband potential V_{FB} = 0.2 ± 0.1 V/NHE for a CCC immersed in 0.5 M K$_2$SO$_4$ solution at pH 6.0, regardless of conversion baths and times.

The previously outlined photoelectrochemical behavior of fresh electrodes was quite independent from the presence or not of ferricyanide in the conversion bath. Differences were observed, in some cases, as for the presence in the photocurrent spectra of the second extrapolation at higher photon energies. The optical bandgap value (E_G = 2.55 ± 0.05 eV at U_E = −1.3 V/SCE) was independent from the presence of ferricyanide as well as from the conversion times ($t \geqslant 30$ s) (see Table I). This finding is evidenced in Fig. 16 where a typical photocurrent spectrum, displaying a unique bandgap value, is reported for a CCC-wf. Such a photocurrent spectrum with a unique extrapolation was frequently found for fresh CCC-wf samples and for conversion times up to 5 min. At the longest conversion times, the usual behavior with two extrapolations in the photocurrent spectra was observed also in the presence of ferricyanide.
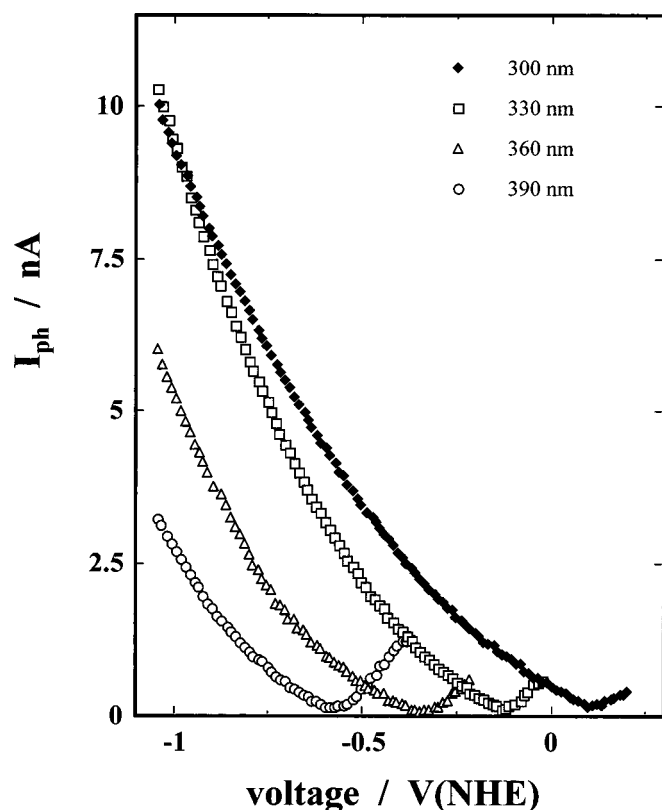

Figure 14. Photocurrent *vs.* potential (v_{scan} = 10 m V/s) plot relating to 60 min CCC-wf on EP-Al, recorded by irradiating the electrode at different wavelengths in 0.5 M K$_2$SO$_4$.
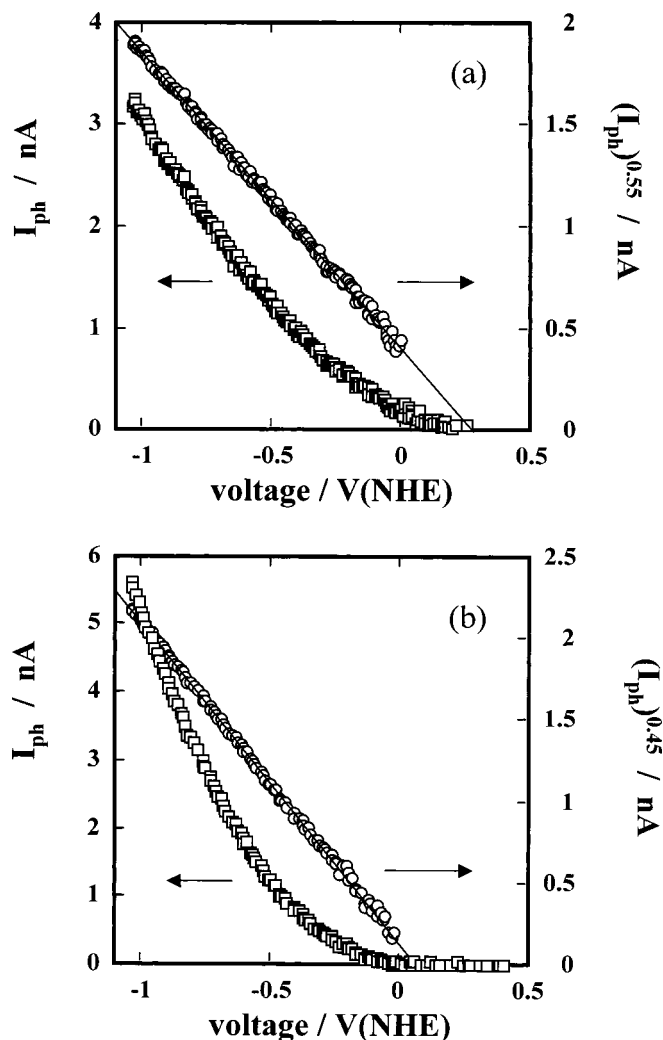

Figure 15. Photocurrent *vs.* potential (v_{scan} = 10 m V/s) plots relating to (a) 5 min CCC-wf on EP-Al (V^* = +0.28 V/SCE and r^2 = 0.999); and (b) 2 min CCC-wof on EP-Al (V^* = +0.07 V/SCE and r^2 = 0.999). Sol: 0.5 M K$_2$SO$_4$. λ = 300 nm.

As previously reported, an influence of the electrode potential on the E_g values was observed on fresh electrodes grown in the presence or absence of accelerator. This is clearly evidenced in the data of Table II pertaining to fresh samples, converted in chromate bath without accelerator, directly polarized from the corrosion potential to the measuring potential U_E.

Discussion

CCC morphology and composition.—The results previously outlined provide considerable information on the structure and composition of a CCC grown on EP-Al samples which allow clarification of some recent and older findings reported in the literature about CCC. The results of Fig. 2 confirm that a continuous very thin (0.6 nm) alumina oxide film is always present during the formation and growth of CCC layer occurring uniformly above the entire Al surface. Moreover, we stress the presence of very fine tunnels inside the CCC extending from the outer surface in contact with the electrolyte to the metal/oxide interface. The presence of such tunnels filled with electrolytic solution (see Fig. 1 and 3) could explain some discrepancies reported in the literature on the CCC composition where the morphology of the layers and thus the inhomogeneity of the composition are not taken into account.
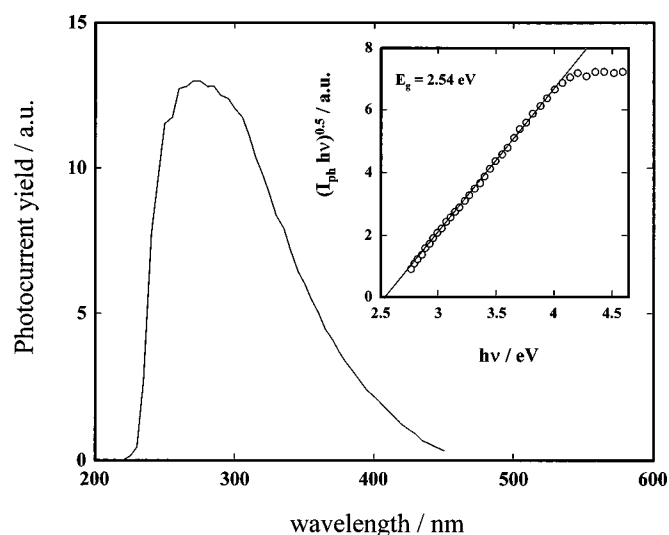
Figure 16. Photocurrent action spectrum corrected for the lamp efficiency, relating to 5 min CCC-wof on EP-Al, polarized in 0.5 M K_2SO_4 at U_e = −1.3 V/SCE. Inset: bandgap determination by assuming nondirect optical transitions.

The TEM and GDOES data analysis allows the conclusion that iron-containing species are present only into the external part of a CCC grown in chromate bath-containing ferricyanide. The thickness of such layer is almost constant (in the order 25-30 nm) for the investigated conversion times according to the EDX and TEM analysis. The difference in the iron content obtained by two techniques probing the local (EDX) or the average (ICP-AES) composition of a CCC is not contradictory when we consider that iron is neatly localized on the exterior of a CCC. The 7 atom % value measured by ICP-AES method agrees with the 20 atom % value of iron determined locally by EDX. Both these concentrations are estimated considering metallic cations only.

The lower concentrated iron species, revealed by GDOES spectra in the inner part of a CCC, could be traced out to the presence of electrolytic solution into the fine tunnels of the coatings as evidenced in the iron mapping of Fig. 3. The lighter appearance (TEM analysis) of the external region of CCC-wf could be attributed to the formation of a less dense layer containing both chromium mixed oxides and chromium-ferro/ferricyanide species.[19,20] The hypothesis of ferricyanide species bonded to chromium hydroxide has been recently suggested[21,22] and is in qualitative agreement with the Cr and Fe GDOES spectra of Fig. 6.

The hypothesis of formation of a Cr(III)-ferro/ferricyanide complex could help to explain the lower Cr(VI) content measured by XANES in CCC-wf. In fact if we assume that CCC-wof for any conversion time contains in a fixed ratio about 1 Cr(VI) for two Cr(III) (see Fig. 8 and 9, and Ref. 6, 10, 23, and 24), it seems reasonable to suggest that when part of Cr(III) is bonded with ferro-ferricyanide species, the formation of mixed [Cr(VI), Cr(III)] oxide is reduced of a corresponding amount.

From XANES data, we get an average (over CE-Al and EP-Al samples) decrease in Cr(VI) of about 4 atom % which implies about 8 atom % of Cr(III) engaged in other bonds. Both the formation of $CrFe(CN)_6$ or $Cr_3[Fe(CN)_6]_4$ are compatible with the XANES and EDX data and the presence of both species have been suggested in the literature.[19,20]

Regarding the mechanism of growth of the CCC, the data of Fig. 4 and 9 are compatible with a growth controlled either by a diffusion-like or an ohmic drop mechanism.[25] The XANES results showing a large influence of the initial surface treatment on the CCC thickness (CCC-wf is only 1.4 times thicker than CCC-wof for EP-Al compared to 2.3 times for CE-Al samples) does not appear compatible with a growth of CCC controlled by a diffusion-like

mechanism. It is also known that the initial surface treatment affects the morphology of CCC grown on Al and Al-alloys.[26]

In the hypothesis of ohmic control it appears reasonable to assume that the active anodic areas and the solution resistance in the fine tunnels and flaws of CCCs are the factors controlling the growth of the layers on Al samples. After an initial transient, a nearly constant corrosion potential (U_{corr} = −0.60 V/SCE) was measured for EP and CE samples during the conversion process. In the case of CE-Al samples, much larger anodic areas and flaws through the CCC can be assumed, with respect to EP-Al samples, in order to explain the larger final thickness measured. The fitting of data of Fig. 9 suggests that a different control operated at shorter times and that the square root dependence holds after a lapse of time (at least around 15 s in Fig. 9) large enough to build a very thick film.

Solid-state properties and energy levels at Al/CCC/electrolyte interface.—The role of the very thin (0.6 nm) oxide layer, existing at the Al/CCC interface, on the rate of growth of the CCC is discussed. The presence of this layer during the CCC formation process seems to exclude any (model of growth of CCC by) direct reaction of Al with electrolytic species. On the other hand its extreme thinness allows easily a tunneling of electronic charge from the underlying metal to the valence band of CCC or directly into the solution, as previously suggested by other[3] authors. This last hypothesis was suggested to explain the CCC growth at the first instants of formation, and contrary to the mechanism of growth initially suggested by Katzman *et al.*[24] Moreover the presence of iron-cyanide species only on the outer part of the film (of almost constant thickness) appears incompatible with a thickening due to a precipitation mechanism and it suggests an inward migration of chromium-containing species as mechanism of growth of a CCC. This outer, possibly very porous, layer could behave as a permeable membrane allowing the ingress of chromium species necessary for CCC thickening. Further investigations at shorter conversion times are necessary to elucidate this aspect.

In order to better evidence the role of electronic processes at different interfaces in the mechanism of growth of a CCC, we need to discuss the PCS results previously outlined. As reported above, the CCCs behaved like insulating (Fig. 14) or slightly p-type semiconducting (Fig. 15) material with bandgap around 2.55 eV (see Tables I and II) and flatband potentials, V_{FB}, close to +0.2 V ± 0.1 V (NHE) at λ = 300 nm and pH $\cong$ 6.0. The presence in the photocurrent spectra of a second extrapolation at higher energy deserves some attention. We return to this aspect at the end of this section after discussing the possible composition of a CCC.

The higher E_g (Table II) measured at more anodic potentials (*i.e.*, at lower band bending), the supralinear behavior of the photocharacteristics and their photon energy dependence (Fig. 15) and the shift of V^* and V_{inv} values with photon energy suggest the existence of traps and localized states within the mobility gap of CCCs. These findings, typical of amorphous materials, can be explained by taking into consideration the field dependence of both optical transitions and transport of photocarriers in localized states.[27-31]

Due to the amorphous nature of CCCs, the presence of electronic states within the mobility gap of the material around the Fermi level, E_F, has been assumed in schematizing the energy levels location (energetics) of CCC/electrolyte junction of Fig. 17. This distribution accounts also for the presence of surface states at the CCC/electrolyte interface. Moreover a shift of the flat band potential of 59 mV/pH, as usual for oxide/aqueous electrolyte interface,[32] has been introduced in Fig. 17 for the location of energy levels in order to reproduce the conditions during the formation of CCC (pH 2; U_{corr} = −0.60 V/SCE). The redox couple Fermi levels in solution have been located according to the redox potentials reported in Ref. 3, 21, 32. According to this Fig. 17 describes the energetics of CCC-electrolyte interface during the growth of CCC (p-type semiconducting) in the cathodic areas of the corroding system where the reduction processes take place.
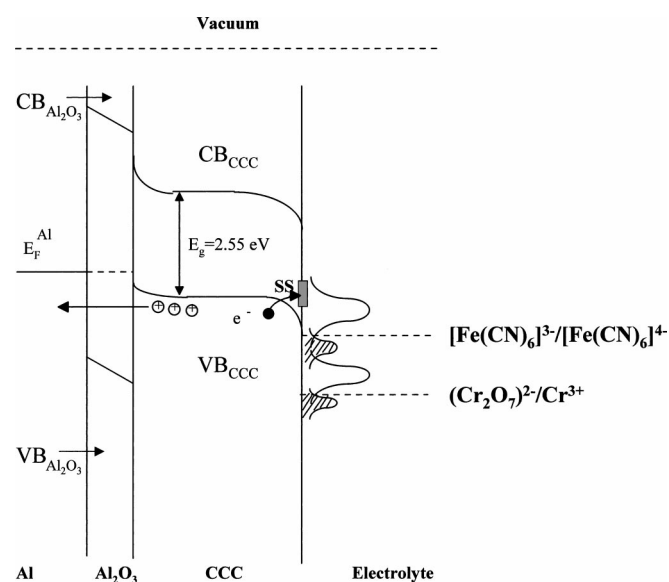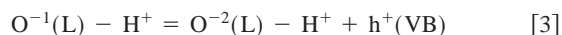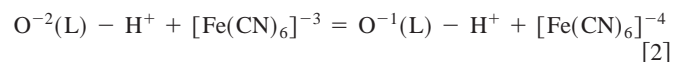
Figure 17. Schematic diagram of substrate/CCC/electrolyte interface during the coating growth ($U_{corr} = -0.6$ V/SCE).

According to Fig. 17 the reduction process of the Cr(VI)/Cr(III) as well as of $[\text{Fe(CN)}_6]^{-3/-4}$ redox couple can occur only by electron exchange with the valence band of CCC. This means that the continuous growth of the CCC is sustained by a mechanism of holes injection into the valence band of CCC at the oxide/electrolyte interface and a contemporary extraction of holes at the inner metal-CCC interface.

In Fig. 17 we assume that holes injection, at the CCC/electrolyte interface containing the accelerator, was mediated by surface states energetically located near the CCC Fermi level, in electronic equilibrium with electronic states of the valence band, and partially overlapping the vacant electronic states in solution of ferricyanide species.

In order to understand the role of accelerators of unielectron redox couples reported in Ref. 21 we need to recall that the Fermi level of the Cr(VI)/Cr(III) redox couple reported in Fig. 17 is not really representative for the kinetics of electron exchange between the CCC and chromium species in solution, because such a redox couple involves a multistep electron exchange and we should have to represent the Fermi levels for each step in order to understand the kinetics of electron exchange.[32] We can conclude that a very slow intermediate step is involved in the reduction of Cr(VI) species in spite of the favorable energetic location of the Fermi level for the overall redox reaction.

By following Morrison,[32] it is reasonable to hypothesize a holes injection mechanism involving the redox couple according to the scheme

$$O^{-2}(L) - H^+ + [\text{Fe(CN)}_6]^{-3} = O^{-1}(L) - H^+ + [\text{Fe(CN)}_6]^{-4} \quad [2]$$

$$O^{-1}(L) - H^+ = O^{-2}(L) - H^+ + h^+(VB) \quad [3]$$

where the hydroxylated surface groups $[O^{-2}(L) - H^+]$ of the CCC play the role of surface states and $h^+(VB)$ indicates a hole in the valence band. According to this scheme, the first equation represents the hole injection process from oxidized species into solution to surface states of the CCC, while the second equation represents the injection of a hole from the surface state into the valence band of the CCC. The capture of holes at the inner interface should occur by electron tunneling across the very thin alumina oxide existing at Al/CCC interface.

By taking into account the solid-state properties of a CCC, the proposed mechanism of electron exchange at the two interfaces could help to better elucidate the influence of different redox couples on the growth rate of the CCC reported previously in literature.[21] It is evident that in order to understand the role of redox couples in accelerating the CCC growth we need to consider both the heterogeneous electronic exchange process, between CCC and redox couples, and the homogeneous electronic exchange between redox couple and dichromate species in solution. In this frame it is evident that rather than the standard potential of the redox couple it is the overall kinetics of electronic exchange in the two processes (homogeneous and heterogeneous) which controls the growth rate of CCC in the presence of accelerator.
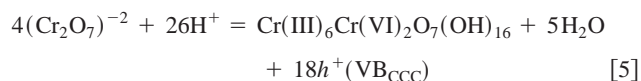
According to this it is not surprising, in the frame of the Marcus theory of electron exchange, that the ferricyanide redox couple is an excellent accelerator for the growth of CCC. It is known from the theory[32] that important parameters for the kinetics of electron exchange are

(*i*) the value of reorganization energy of a redox couple in solution; and

(*ii*) the energy levels of electronic states in solution with respect to the electronic surface states of the oxide electrode.

It seems very probable that both these parameters are more favorable for the ferri-ferrocyanide redox couple than for other redox couples reported in Ref. 21. Further investigations on the kinetics of electron exchange between CCC and redox couples in solution are necessary for a better understanding of the role of different redox couples, but it seems to us that the previous suggestions could help to rationalize the experimental findings.

According to the previous suggestions, the thinning of the surface oxide by fluoride ions is an important step at the beginning of CCC growth.[3] However, after the initial formation of the CCC layer the continuous growth of the CCC was controlled by the coupled processes of Al^{3+} transport, trough fine tunnels and flaws present on CCC, and holes injection at the CCC/electrolyte interface. In such a hypothesis, the anodic and cathodic processes can be summarized as

$$6Al + 18h^+(VB_{CCC}) = 6Al^{3+}(\text{solution}) \quad [4]$$

$$4(Cr_2O_7)^{-2} + 26H^+ = Cr(III)_6Cr(VI)_2O_7(OH)_{16} + 5H_2O$$
$$+ 18h^+(VB_{CCC}) \quad [5]$$

where the anodic process accounts for the Al^{3+} ions formation by hole injection at the metal/CCC interface, while the cathodic process accounts for the formation of a Cr(VI)-Cr(III) mixed oxyhydroxide. In the absence of accelerator the injection of hole into CCC occurred according to Eq. 5 (slow process) while in presence of accelerator (ferricyanide redox couple) a second reaction channel for the hole injection was provided by Eq. 2 and 3. In this case, the ferrocyanide species was subsequently oxidized by dichromate species presents in solution.

The chemical composition reported in Eq. 5 is analogous to that suggested in Ref. 4 for a Cr(VI)/Cr(III) ratio equal to 1:3 for explaining the self-healing effect of Cr(VI) species. The possible presence of crystallization water in the CCC formation has not been taken into account because its presence will not affect the bandgap of the CCC (see below).

Estimate of CCC composition through PCS data analysis.—It is interesting to note that Eq. 4 and 5 are able to fit different Cr(VI)/Cr(III) ratios and hydroxylation degree as a function of the number of dichromate groups involved in the reaction. If we assume that only three dichromate groups are involved in the growth process of a CCC we get a ratio Cr(VI)/Cr(III) = 1:2 analogous to the average ratio above reported from XANES measurements for EP-Al electrodes.

In order to support the hypothesis of formation of chromium (VI, III) mixed oxide, we take advantage of the PCS data showing that, regardless of conversion times and bath, a quite reproducible optical

bandgap value, around 2.55 eV, is derived for a fresh CCC. Such a value is appreciably different from that measured for passive chromium and attributed to $Cr(OH)_3$ anodic film (2.40 eV).[16] More importantly, the measured E_g values must be relative to a compound containing about 1/3 of Cr(VI) species. In the following, we present a quantitative PCS data analysis which support the hypothesis that an amorphous Cr(III)-Cr(VI) mixed oxyhydroxide is the main constituent of CCC formed in the absence of accelerator. The presence of chromium-iron-cyanide species in the outer layer of CCC-wf does not affect appreciably our reasoning.

In order to accomplish such a task we make use of correlation between bandgap and oxide film composition recently proposed in the literature.[12,33-36] According to such studies, the bandgap of crystalline oxide can be estimated according to equation

$$E_g(eV) = A(\chi_O - \chi_M)^2 + B \qquad [6]$$

where χ_O and χ_M are the Pauling's electronegativity of oxygen and metallic cation respectively and $A = 1.35$ and $B = -1.49$ for d-metal crystalline oxides. It has been shown[34,35] that such a correlation holds also for amorphous oxides once a correcting term, $\Delta E_{am} = 0.1 \div 0.35$ eV, is added to the E_g values for taking into account the influence of lattice disorder on the bandgap of the corresponding crystalline counterpart.

In the case of ternary mixed oxides $A_a B_b O_c$, Eq. 6 still holds after substituting to χ_M, an average cationic electronegativity defined as

$$\chi_{c,av} = (x_A \chi_A + x_B \chi_B) \qquad [7]$$

$$x_A = \frac{a}{a + b} \qquad [8]$$

where χ_A and χ_B represents the electronegativity value of cations A and B and x_A and x_B their respective cationic fraction in the mixed oxide.

In order to get the average electronegativity parameter we need to know the electronegativity value of Cr(VI). At this aim we make use of Eq. 6 and of the value of 2.0 eV reported in the literature for the bandgap of CrO_3 crystalline oxide.[37] By substitution of this E_g value in Eq. 6 and by using 3.5 for the electronegativity of oxygen, we get $\chi_{Cr(VI)} = 1.89$. The higher Cr(VI) electronegativity, with respect to Cr(III) ($\chi = 1.6$), is in accordance with the usually reported trend for increasing oxidation number of the elements (Ref. 33 and references therein). We are not aware of other values for the electronegativity parameter of Cr(VI) so that we use it with some caution.

According to Eq. 7 and 8 we calculate $\chi_{c,av}$ as a function of the Cr(VI)/Cr(III) ratio. By assuming for such a ratio an average value equal to 1:2 (in agreement with our XANES data) we define an average cationic electronegativity parameter for the metallic group in CCC: $\chi_{c,av(CCC)} = 1.697$.

In order to estimate the bandgap of crystalline mixed Cr(VI, III) oxide we make use again of Eq. 6 and of the average cationic electronegativity parameter obtaining $E_g = 2.90$ eV. By taking into account the amorphous nature of a CCC, we can assume reasonably an average ΔE_{am} value of 0.20 eV, which poses the optical bandgap for anhydrous amorphous CCC close to 3.10 eV. The assumed $\Delta E_{am} = 0.20$ eV is in agreement with the difference of E_g values between amorphous (3.55 eV) and crystalline (3.35 eV) Cr_2O_3 oxide[16] although a higher value of such parameter like for other oxides[34,35] is not unreasonable.

The measured E_g value of a fresh CCC is well below this value and according to Refs. 12, 33-37 could be related to the formation of a mixed hydroxide phase. In fact, in the case of d-metal hydroxides, lower E_g[35,36] have been estimated according to the correlation

$$E_g(eV) = 0.65(\chi_M - \chi_{OH})^2 + 1.38 \qquad [9]$$

where χ_{OH} represents now the electronegativity parameter for the OH group. By using the average values of electronegativity for the cationic (1.696) and anionic (2.85) groups respectively, we get an estimate for the optical bandgap of chromium (VI, III) mixed hydroxide as 2.25 eV.

These preliminary analysis suggests, in agreement with previously reported findings on passive films grown on different metals,[16,33,38,39] that the optical bandgap values of CCC differs from the estimated values of pure amorphous oxide (3.10 eV) as well as of pure hydroxide (2.25 eV) and that a mixed Cr(VI,III) oxyhydroxide is formed during the chemical conversion process.

In previous works[33,36,38] we suggested that in the case of mixed oxyhydroxide, passive films of general formula $MO_{(y-m)}OH_{2m}$ (with m ranging between 0 and y), an estimate of the bandgap value for such a compounds can be obtained by using the following connection formula

$$E_g = \frac{E_g^{anh}}{1 + k_M x_{OH}} \qquad [10]$$

where $x_{OH} = 2m/(y + m)$ is the hydroxylation degree, E_g^{anh} is the bandgap of anhydrous oxide, and k_M is a constant, for each metal oxyhydroxide, which can be derived once the bandgap of the oxide ($x_{OH} = 0$) and of the hydroxide ($x_{OH} = 1$) are known. In our case after substitution of the E_g values for amorphous oxide and hydroxides in Eq. 10 we find for $k_{Cr(VI,III)}$ a value of 0.378.

By substituting in Eq. 10 to $E_g(x_{OH})$ the value measured for CCC (2.55 eV), we get finally the value of $x_{OH} = 0.57$ from which $m = 0.80$ is derived. From such a value of m we can get a mixed oxyhydroxide ($Cr_{.667}Cr_{.333}O_{1.2}(OH)_{1.6}$) having a stoichiometric ratio O/Cr equal to 2.80. This last value is in fair agreement with data reported in literature and measured by Auger spectroscopy.[2] Analogous results were obtained by using instead of Eq. 10 a slightly different approach, always based on E_g data analysis, reported in Ref. 39.

By assuming a ratio $Cr^{III}:Cr^{VI} = 2:1$, we obtain from Eq. 5 a reduced stoichiometric formula: $Cr_{.667}Cr_{.333}O_{1.17}(OH)_{1.67}$ to which corresponds an optical bandgap of 2.53 eV in very good agreement with the experimental value measured for our CCC. It seems reasonable to conclude that the composition of CCC, grown on EP-Al electrodes in the conversion baths used for this work, is very close to the polymeric compound proposed by Mc Creery but with a ratio of $Cr^{III}:Cr^{VI}$ equal to 2:1.

It may be of interest to calculate the bandgap expected for the compound proposed by Mc Creery *et al.* and reported in Eq. 5 without taking into consideration the water of crystallization. By following the same procedure we estimated an optical bandgap value of 2.50 eV which is not too far from our value. The reason for this almost invariant value of E_g in presence of a different Cr(VI)/Cr(III) ratio, comes out from the fact that in the compound of Eq. 5 proposed by Mc Creery *et al.* an increase in the content of Cr(III), which increased the bandgap value of anhydrous a-CCC up to 3.22 eV, is overcompensated by the increase of OH groups content which lowered the bandgap to the estimated 2.5 eV.

According to our interpretative hypothesis it comes out from the data of Table I that the optical bandgap values of fresh CCC grown on EP-Al electrodes are compatible with an amorphous polymeric phase of generic formula $Cr_4(Cr_2O_7)O_n(OH)_{10-2n}$ with n ranging between zero and 1.

A decrease in the hydroxilation degree, from the CCC/solution interface toward the inner layers, could account for the presence of a second extrapolation, at higher energy, in the photocurrent spectra of CCC. As above mentioned (see also Fig. 12, 13, 16) such a second threshold was usually observed in CCC-wof but rarely for CCC-wf and usually for longer conversion times (thicker films).

A possible explanation for the absence of a second extrapolation could be the presence of a thicker (or rougher and then optically thicker) hydroxylated layer on the surface of CCC-wf above a less

hydroxylated internal layer: only the external layer should detected in this case. In the case of CCC-wof, both layers are detected and the photocurrent spectra exhibit two slopes. Such an interpretation is in agreement with results previously reported in the literature on layered passive films having a variable hydroxylation degree.[16,38-40]

Conclusion

The use of different techniques has allowed to get new insights on the morphology, structure, and composition of CCCs grown on pure aluminum samples. The results obtained on pure aluminum electrodes confirm the presence of iron species only on the external part of the coatings formed in conversion bath containing ferricyanide. Such iron distribution seems independent from the coating times. Our results seem to suggest that iron is present as a complex containing both cyanide group and Cr(III) species. More importantly, the presence of fine tunnels within the CCC could account for some discrepancies reported in literature on CCC composition. It is suggested that such tunnels represent the anodic areas and are the preferential paths for the outcome of Al^{3+} species during the coating formation process. Such a hypothesis could account for the lack of appreciable amount of aluminum in the CCC composition.

The XANES data of this work and the PCS study agree with the hypothesis that a mixed oxyhydroxide of Cr(III) + Cr(VI) is formed during the conversion process. The exact composition of the CCC depends on both the surface preparation and the bath composition. The optical bandgap of 2.55-2.60 eV obtained for the CCC is compatible with an average coating composition of $Cr_4(Cr_2O_7)O_n(OH)_{10-2n}$ ($0 \leqslant n \leqslant 1$). The presence in the photocurrent spectra of a second absorption threshold, at high photon energies, has been related to the presence of a less hydroxylated inner layer. The absence of this second threshold, in some of the samples formed in presence of ferricyanide, could be related to the presence on such samples of an optically thicker outer hydroxylated layer. The PCS data suggest that CCC grown on pure Al present an insulator-like or slightly p-type behavior.

These results as well as the TEM morphological analysis seem to suggest that the presence of ferricyanide in the conversion bath plays a more complex role than a simple accelerator of growth kinetics.

A general electrochemical reaction scheme has been proposed for the coating conversion process by taking into account both the solid-state properties of CCC as well as the possible mechanisms of charge injection at the different interfaces. In this frame, a rationalization of the influence of redox couples on the growth rate of CCC has been suggested by taking into consideration the kinetics of electron exchange at the CCC/electrolyte interface. More detailed studies on these kinetics are, however, necessary before reaching a final conclusion.

Finally, it has been shown that PCS technique can be used in a quantitative way to identify the photoactive layer once some preliminary information are gathered by other techniques. Further studies are now in progress to understand the influence of aging process on the physicochemical properties of CCC.

References

1. J. A. Treverton, M. P. Amor, and A. Bosland, *Corros. Sci.,* **33**, 1411 (1992).
2. F. W. Lytle, R. B. Greegor, G. L. Bibbins, K. Y. Blohowiak, R. E. Smith, and G. D. Tuss, *Corros. Sci.,* **37**, 349 (1995).
3. G. M. Brown, K. Shimizu, K. Kobayashi, G. E. Thompson, and G. C. Wood, *Corros. Sci.,* **34**, 1045 (1993); K. Shimizu, G. M. Brown, K. Kobayashi, G. E. Thompson and G. C. Wood, *Corros. Sci.,* **34**, 1853 (1993).
4. L. Xia and R. L. McCreery, *J. Electrochem. Soc.,* **145**, 3083 (1998).
5. J. D. Ramsey and R. L. McCreery, *J. Electrochem. Soc.,* **146**, 4076 (1999).
6. A. J. Davenport and H. S. Isaacs, *Corros. Sci.,* **31**, 105 (1990); M. W. Kendig, A. J. Davenport and H. S. Isaacs, *Corros. Sci.,* **34**, 41 (1993).
7. J. Zhao, G. S. Frankel, and R. L. McCreery, *J. Electrochem. Soc.,* **145**, 2258 (1998).
8. C. S. Jeffcoate, H. S. Isaacs, A. J. Aldykiewicz Jr., and M. P. Ryan, *J. Electrochem. Soc.,* **147**, 540 (2000).
9. L. Xia, E. Akiyama, G. S. Frankel, and R. L. Mc Creery, *J. Electrochem. Soc.,* **147**, 2556 (2000).
10. V. Laget, H. S. Isaacs, C. S. Jeffcoate, and R. G. Buchheit, *ATB Metall.,* **40-41**, 295 (2000, 2001); V. Laget, H. S. Isaacs, C. S. Jeffcoate, and R. G. Buchheit, in *Corrosion and Corrosion Control in Saltwater Environments*, P. M. Natishan, S. Ito, D. A. Shifler, and T. Tsuru, Editors, PV 99-26, p. 173, The Electrochemical Society Proceedings Series, Pennington, NJ (1999).
11. L. Anicai, S. Piazza, M. Santamaria, C. Sunseri, and F. Di Quarto, *ATB Metall.,* **40-41**, 175 (2000, 2001).
12. F. Di Quarto, C. Sunseri, S. Piazza, and M. Santamaria, *Handbook of Thin Films*, H. S. Nalwa Editor, Vol. 2, p. 373, Academic Press, New York (2002).
13. N. J. Newhard, *Met. Finish.*, **1972**, 49 (July).
14. S. Piazza, A. Splendore, A. Di Paola, C. Sunseri, and F. Di Quarto, *J. Electrochem. Soc.,* **140**, 3146 (1993).
15. R. C. Furneaux, G. E. Thompson, and G. C. Wood, *Corros. Sci.,* **18**, 853 (1978).
16. F. Di Quarto, S. Piazza, and C. Sunseri, *Corros. Sci.,* **31**, 721 (1990); C. Sunseri, S. Piazza, F. Di Quarto, *J. Electrochem. Soc.,* **137**, 2411 (1990).
17. P. Schmuki, M. Buchler, S. Virtanen, H. Bohni, R. Muller, and L. J. Gauckler, *J. Electrochem. Soc.,* **142**, 3336 (1995).
18. Yu. Ya Gurevich, Yu. V. Pleskov, and Z. A. Rotenberg, *Photoelectrochemistry*, Consultants Bureau, New York (1980).
19. J. A. Treverton and N. C. Davies, *Met. Technol. London,* **4**, 480 (1977); J. A. Treverton and N. C. Davies, *Surf. Interface Anal.,* **3**, 194 (1981).
20. A. E. Hughes, R. J. Taylor, and B. R. W. Hinton, *Surf. Interface Anal.,* **25**, 223 (1997).
21. L. Xia and R. L. McCreery, *J. Electrochem. Soc.,* **146**, 3696 (1999).
22. L. Juff, A. E. Hughes, S. Furman, and P. J. K. Paterson, *Corros. Sci.,* **44**, 1755 (2002).
23. J. Wan, G. E. Thompson, K. Lu, and C. J. E. Smith, *Physica B*, **208, 209**, 511 (1995).
24. H. A. Katzman, G. M. Malouf, R. Bauer, and G. W. Stupian, *Appl. Surf. Sci.,* **2**, 416 (1979).
25. E. Akiyama and G. S. Frankel, *J. Electrochem. Soc.,* **146**, 4095 (1999).
26. P. Campestrini, E. P. M. van Westing, and J. H. W. de Wit, *Electrochim. Acta,* **46**, 2553 (2001).
27. F. Di Quarto, S. Piazza, R. D'Agostino, and C. Sunseri, *J. Electroanal. Chem. Interfacial Electrochem.,* **228**, 119 (1987).
28. F. Di Quarto, S. Piazza, and C. Sunseri, *Electrochim. Acta,* **38**, 29 (1993).
29. H. Gerischer, *Corros. Sci.,* **29**, 257 (1989); H. Gerischer, *Corros. Sci.,* **31**, 81 (1990).
30. N. F. Mott and E. A. Davis, *Electronic Processes in Non-crystalline Materials*, 2nd ed., Clarendon Press, Oxford, U.K. (1979).
31. G. D. Cody, *Semiconductors and Semimetals*, Vol. 21 B, J. I. Pankove, Editor, Academic Press, New York (1984).
32. S. R. Morrison, *Electrochemistry of Semiconductor and Oxidized Metal Electrodes*, Plenum Press, New York (1980).
33. F. Di Quarto, C. Sunseri, S. Piazza, and M. C. Romano, *J. Phys. Chem. B*, **101**, 2519 (1997).
34. M. Santamaria, D. Huerta, S. Piazza, C. Sunseri, and F. Di Quarto, *J. Electrochem. Soc.,* **147**, 1366 (2000).
35. Di Quarto, M. Santamaria, S. Piazza, and C. Sunseri, *Symposium AA Structure-Property Relationships of Oxide Surfaces and Interfaces*, C. B. Carter, X. Pan, K. Sickafus, H. L. Tuller, and F. T. Wood, Editors, Vol. 654, p. AA4.8.1, Materials Research Society Proceedings, Warrendale, PA (2001).
36. F. Di Quarto, M. C. Romano, M. Santamaria, S. Piazza, and C. Sunseri, *Russ. J. Electrochem.,* **36**, 1203 (2000).
37. P. A. Cox, *Transition Metal Oxides*, p. 105, Clarendon Press, Oxford, U.K. (1992).
38. S. Piazza, S. Caramia, C. Sunseri, and F. Di Quarto, in *Passivity and Localized Corrosion*, M. Seo, B. MacDougall, H. Takahashi, and R. G. Kelly, Editors, PV 99-27, p. 317, The Electrochemical Society Proceedings Series, Pennington, NJ (1999).
39. C. A. Moina and G. O. Ybarra, *J. Electroanal. Chem.,* **504**, 175 (2001).
40. F. Di Quarto, S. Piazza, C. Sunseri, M. Yang, and S. M. Cai, *Electrochim. Acta,* **41**, 2511 (1996).